Article

Not peer-reviewed version

Handling Microstructural Changes and Hardness of the AlSi10Mg Alloy Through SC Doping and Direct Aging Treatment

Fellipe Martinez , Carlos Dos Santos Junior , Jaderson Leal , Argos Silva , Guilherme Gouveia , Jose Spinelli *

Posted Date: 8 March 2023

doi: 10.20944/preprints202303.0141.v1

Keywords: AlSi10Mg; Scandium; microstructure; direct aging; hardness

Article

Handling Microstructural Changes and Hardness of the AlSi10Mg Alloy through SC Doping and Direct Aging Treatment

Fellipe Martinez [1], Carlos dos Santos Junior [1], Jaderson Leal [2], Argos Silva [2], Guilherme Gouveia [2] and José Spinelli [1,2,*]

[1] Department of Materials Engineering, Federal University of São Carlos UFSCar, 13565-905 - São Carlos, SP, Brazil
[2] Federal University of São Carlos, Graduate Program in Materials Science and Engineering, 13565-905 - São Carlos, SP, Brazil
* Correspondence: spinelli@ufscar.br

Abstract: The effects of 0.4wt.% Sc addition on a typical Al-Si10-Mg alloy were systematically investigated in the present research. Samples with and without Sc produced refined dendritic arranged microstructures with sensitivity to the aging treatment after solidification, particularly in the case of the alloy without Sc. After being exposed to 300°C for 90 minutes, the dendritic spacing nearly doubled in the Al-10wt.%Si-0.45wt.%Mg samples. The rapidly solidified microstructures were constituted by the -Al dendritic phase surrounded by eutectic phases/intermetallics such as Si, Mg_2Si and Al_3Sc (in the case of the alloy containing Sc). 255°C and 300°C were deemed most appropriate temperatures for aging treatments, with four exposure times of up to 120 minutes tested for each alloy. The heat treatments allowed the Vickers hardness profiles to be plotted and compared. Moreover, in order to detect both Sc- and Mg- precipitates after aging, specific samples have been prepared for either SEM or TEM analyses. At first, the results pointed to a strong precipitate-related hardening effect formed as a result of the Sc addition to the alloy. All samples containing Sc showed a higher hardness value when compared to their respective treated samples without Sc. Secondly, when comparing the Al-10Si-Mg-Sc alloy samples among themselves after being treated at different conditions, high temperatures and excessive treatment times can become detrimental to the hardness. This was due to the growth of larger Sc-bearing precipitates of approximately 1 μm in size under such conditions, having less pronounced hardening effect. The best condition (255°C for 60 min) for as centrifuged samples in Cu-mold produced very fine dispersion of Mg- and Sc- intermetallics (~200 nm in size) with a peak hardness of 110 HV.

Keywords: AlSi10Mg; Scandium; microstructure; direct aging; hardness

1. Introduction

Al-Si-Mg alloys combine the decrease in melting temperature, solidification interval, and thermal shrinkage, as well as the increase in fluidity resulting from the addition of Si, with the ability to increase mechanical strength generated by precipitation hardening provided by the association of small amounts of Mg and proper heat treatment, enabling the application of these alloys in structural components [1,2]. This combination of properties gives the Al-Si-Mg alloys high versatility of applications in the aerospace, aeronautical, and automotive industries [3,4].

The AlSi10Mg alloy emerges among the alloys in this system for high-performance applications due to its combination of high specific strength, suitable electrical conductivity, high corrosion resistance, adequate weldability, and limited solidification interval [1,5]. Such distinct set of properties enables the AlSi10Mg alloy to be used in a variety of processes ranging from traditional

 doi:10.20944/preprints202303.0141.v1

casting to additive manufacturing (AM) such as selective laser melting (SLM), high-pressure die casting (HPDC), and permanent mold casting (PM) [3,4] for an even broader range of applications.

Aiming to further improve the properties of the AlSi10Mg alloy in terms of the intrinsic properties of the alloy or ways to improve the properties resulting from a specific processing, some modifications can be performed. One example is the addition of hexaboride nanoparticles such as CaB_6, CeB_6, NdB_6, with emphasis on LaB_6, in order to reduce the columnar grain growth and, consequently, the anisotropy of the mechanical properties resulting from selective laser melting (SLM) processing [6]. Many studies have been conducted in order to meet new technological demands, with the goal of adding new alloying elements, ceramic particles, and heat treatments [7–10].

Commonly, in Al alloys intended for casting, elements are added so that a supersaturated solution could be formed after the solidification process at sufficiently high solidification rates. From this unstable state, when these alloys undergo adequate heat treatment, a dispersion of refined precipitates is formed along the α-Al matrix, providing an increase in mechanical resistance if adequate treatment conditions are performed [11]. More specifically for the AlSi10Mg alloys, it is possible to highlight in the literature the following added elements fulfilling this role: Cu, Zr, Ce, Er, and Sc, which work cooperatively with Mg. The respective precipitated intermetallics formed from these elements are Al_2Cu, Al_2CuMg, Al_3Zr, $Al_{11}Ce$, Al_3Er, Al_3Sc, and Mg_2Si [3,4,11,12]. As demonstrated by Peng et al. [4] the use of multi-micro additions of elements, in the case of Er and Zr, can lead to results that are significantly superior to those obtained by the micro-addition of either Er or Zr.

Another approach for cast alloys is the addition of alloying elements whose function is to change the morphology of the phases present in the microstructures to shapes more favorable to improve mechanical performance, particularly ductility. One example is Sr addition to morphologically modify the eutectic Al-Si microconstituent and the other phases containing Fe and Mg. Another example is the use of Mn to change the morphology of intermetallic phases containing Fe, which typically have a needle-like shape that provides stress concentrators, to more favorable structures of Chinese script or skeletal types [13]. It is also worth mentioning the use of elements for the purpose of grain refinement [6,13].

In the present study, Sc was chosen as a microaddition element in the AlSi10Mg alloy. This element may act in grain refinement due to the formation of the Al_3Sc intermetallic, which is the same that can be formed for hardening through heat treatment [2]. Supersaturation of Sc in the α-Al matrix is only obtained at solidification cooling rates higher than 10 K/s [12]. The low solubility associated with the low diffusivity of Sc, which on the one hand provides the thermal stability of this phase, on the other hand, makes the production of the supersaturated state disadvantageous through the heat treatment of homogenization followed by quenching [12]. The potential improvements in mechanical properties caused by the addition of Sc are restricted by its high cost, making even clearer the need for studies aimed at optimizing the addition procedures for this element [12].

Therefore, a proper understanding of the solidification processing, phase formation, and heat treatments is necessary in order to optimize the properties of AlSi10Mg alloys. As an example, we can cite the negative effects on shrinkage and gas porosity caused by the occurrence of Sr, or the possibility of the formation of ternary AlCeSi intermetallics with needle-like morphologies, and consequently harmful to the mechanical properties, caused by the addition of Ce [11]. According to these insights and the prospects on the alloy enhancement, the current study aims to improve understanding of the heat treatment of the AlSi10Mg alloy with 0.4 wt.% Sc addition.

2. Materials and Methods

One of the experiment's objectives of the performed was to check the impact of the centrifugal cast processing on the as-cast microstructures of the Al-10%Si-0.45%Mg- 0.4%Sc and Al-10%Si-0.45%Mg alloys. Another goal was to investigate the effects of adding Sc or varying the aging treatment time and temperature on the microstructure (dendritic microstructure length-scale and phases formed), as well as to directly age the rapid solidified samples of both alloys without the

Preprints (www.preprints.org) | NOT PEER-REVIEWED | Posted: 8 March 2023 doi:10.20944/preprints202303.0141.v1

solution treatment step. The Vickers hardnesses of these alloys after direct aging were also examined and compared.

The alloys were produced using commercially pure Al, Mg, and Si, together with an Al-10wt.% Si-0.4wt.% Sc master alloy. In order to achieve the required chemistries for the production of the centrifuged samples, charge balance of these elements was performed for both Al-10wt.% Si-0.45wt.% Mg- 0.4wt.% Sc and Al-10wt.% Si-0.45wt.% Mg alloys, considering type plate samples thicknesses of 4.0 mm. Before cast the samples through centrifugal in Cu mold, both alloys were produced through melting the elements in a Zr oxide-coated crucible using an induction furnace, Inductotherm, VIP Power-Trak model, with a power source of 50 kW and a frequency of 3.2 kHz. Al-10%Si-0.45%Mg-0.4%Sc alloy was produced by only adding Mg to the master alloy that was anticipated. It should be emphasized that the two alloys underwent a degassing process with argon for 2 min before being poured into the mold, preventing the retention of gases during the solidification process.

In a hermetic chamber that was positioned perpendicular to a spinning axis in the centrifugal casting apparatus, both alloys were cut, cleaned, and inductively melted (Linn High Therm, Titancast 700 VAC model). During operation, the molten alloy was propelled into the Cu mold cavity by the force created by the chamber's rotation (400 rpm). At relatively high solidification rates, samples of both alloys with 4 mm thick plate geometry were produced. The solidification conditions were the same for both alloys examined. Figure 1 shows the information on the Cu-mold, cast plate dimensions, the aging process, and microstructural characterization.

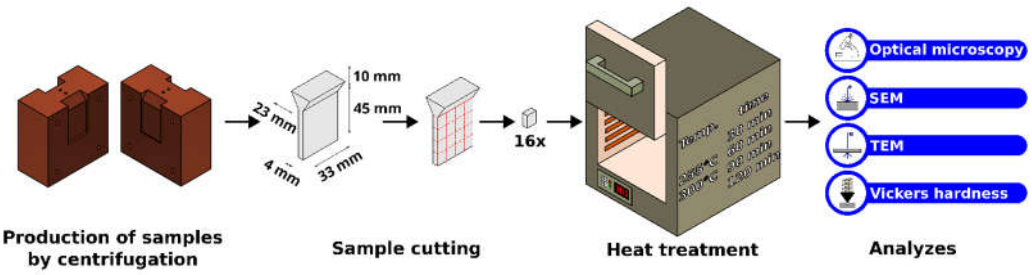

Figure 1. Schematic illustration of the generated samples through centrifugal casting, samples size, heat treatment conditions, and characterization methods employed.

The cast plates of both alloys were cut to generate samples for the direct aging treatments with the following parameters: temperatures of 255°C and 300°C for times 30 min, 60 min, 90 min, and 120 min. A muffle EDG furnace (10P-5 model) was used for these treatments.

To disclose the dendritic arrangement, all cast and aged samples were mounted, ground, polished, and etched with a Keller solution (HF 1%; HCl 1.5%; HNO3 2.5%) for approximately 5 seconds. The secondary, λ_2, dendritic spacings were measured using the intercept method after the images were taken with an optical microscope (Olympus, BX14 M-LED). X-ray diffraction (XRD) measurements were performed, in a 2θ 20-90° interval, using Kα-Cu radiation with a wavelength of 1.5406 Å.

Vickers hardness tests of the as-cast and as-aged samples were performed using a 1 kgf test load and a dwell time of 15 seconds. The representative hardness value for each sample/condition was determined by taking the average of at least 10 measurements.

A scanning electron microscope (SEM) equipped with an energy-dispersive spectrometer was used to investigate the formation of Sc-containing intermetallics in the Al-Si-Mg-Sc alloy samples.

In order to investigate the formation of submicrometric Sc- intermetallics possibly formed during aging treatment, slices of ~500 μm were sectioned from the Al-Si-Mg-Sc samples treated aged at 300°C/120 min and at 255°C/60 min using a precision cutter. These slices were ground, on both sides, to a thickness of ~60 μm. Once the desired thickness was obtained, 3 mm diameter discs were extracted from the slices using a disc punch. Right before STEM observation, the samples were polished using a Precision Ion Polishing System (PIPS) for final thinning and cleaning of the sample surface.

Preprints (www.preprints.org) | NOT PEER-REVIEWED | Posted: 8 March 2023 doi:10.20944/preprints202303.0141.v1

High-resolution characterization conducted by STEM analyses was done in an FEI TECNAI G2 F20 HRTEM equipment, which is a TEM equipped with a FEG electron gun, electron acceleration voltage of 200 kV, energy dispersive spectrometer (EDS) and a high-angle annular dark field (HAADF) detector, among other functions. Scan transmission electron microscopy (STEM) function, together with EDS equipment, was used to obtain elemental mapping images of the elements Al, Si, Mg, Fe, and Sc, in order to observe the particles of these elements, in particular the Sc particles, present in the samples of the Al-10% Si-0.45% Mg-Sc alloy aged at 300°C for 120 min and 255° C for 60 min. The HAADF detector was also used in this analysis to obtain images of the samples with atomic weight contrast, thus allowing for easier visualization of the regions with a higher concentration of heavy elements.

3. Results and discussions

3.1. Thermal analyses and aging temperature for the Sc-containing alloy

The ideal aging temperature for Al alloys containing Sc, according to Marquis et al. [14], should be close to 300°C. Although the aging tests were carried out at this temperature, a different one should be established for comparison purposes. AlSi10Mg-Sc alloy powder samples have been used in a detailed DSC examination to support the establishment of another temperature. As such, DSC analysis was performed on the powder (< 125 μm) samples to monitor the heat flux variation during the aging operation. About 20 mg of powders were weighed and put into a 200 F3 Maia DSC device. Nitrogen was used as the shielding gas. Samples were ramped to 350°C at a rate of 15K/min, maintained for 20 minutes, and cooled back to room temperature at 60K/min.

The DSC results can be seen in Figure 2. It was possible to see a change in the DSC curve at the temperature around 255°C, during the heating step, which indicated the precipitation of phases of interest in the analyses with a threshold at 350°C. If no microstructural change occurs, a smooth curve should be observed, which is not the case here. An exothermic heat flux can be observed starting at 255°C and ending at 290°C. Based on that, the second aging temperature for this investigation was 255°C, within this range.

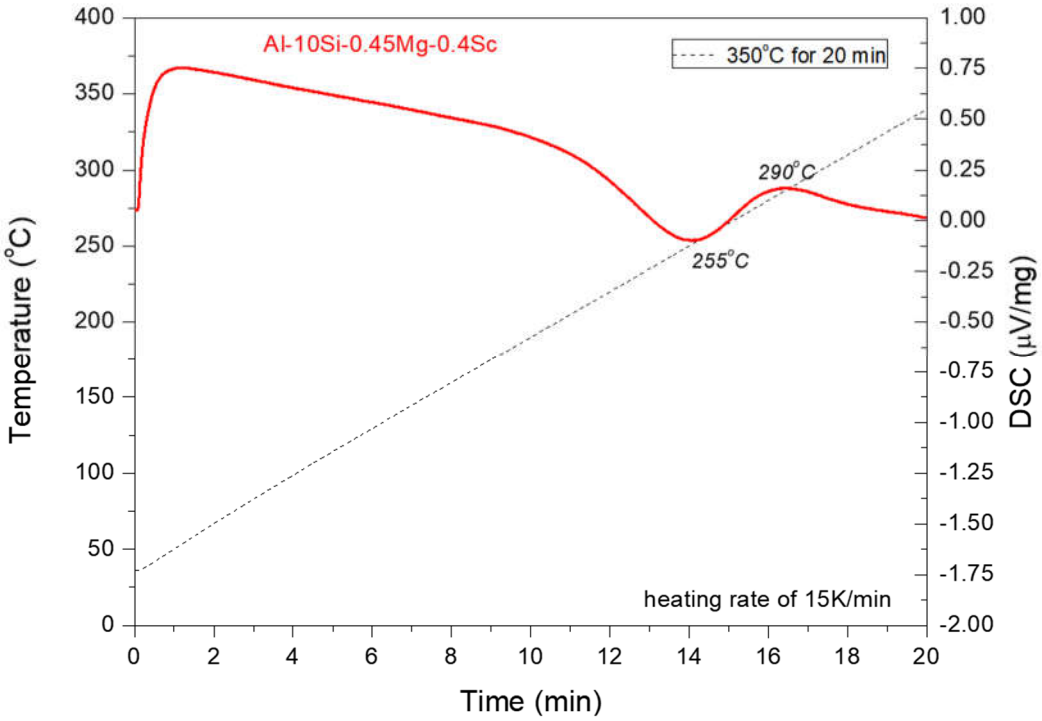

Figure 2. DSC curve for AlSi10Mg0.4Sc powders with <125 μm size range.

Preprints (www.preprints.org) | NOT PEER-REVIEWED | Posted: 8 March 2023 doi:10.20944/preprints202303.0141.v1

3.2. Dendrite arm spacing (DAS)

When the melt cools down, Al-rich dendrites form first as can be seen in both Figures 3 and 4. Between the Al-rich dendritic networks (lighter areas), eutectic constituents composed of Al-rich+Si+Mg_2Si and Al-rich+Si+Mg_2Si+Al_3Sc phases (darker areas) form for the Al-Si-Mg and Al-Si-Mg-Sc alloys, respectively.

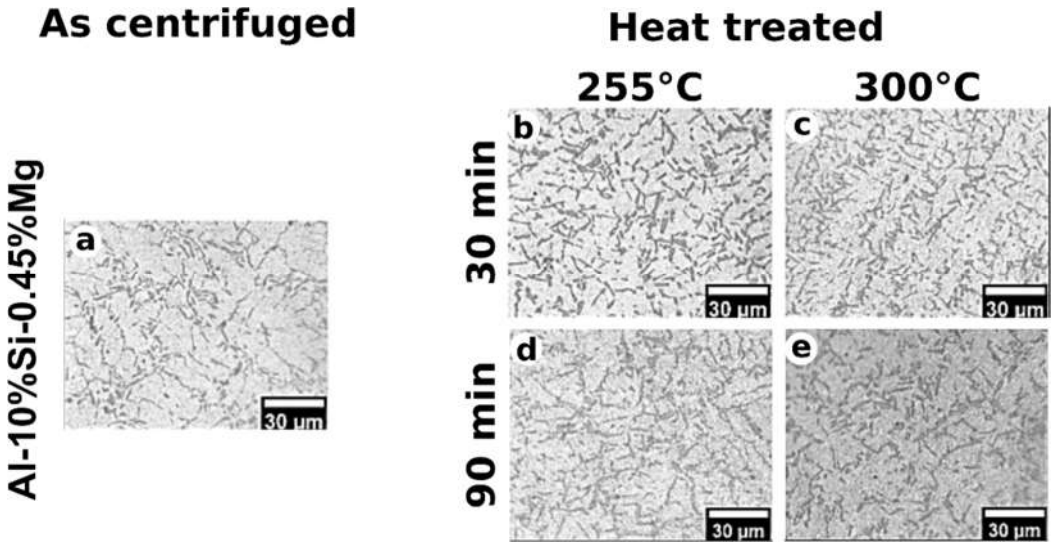

Figure 3. Representative microstructures of the Al-10%Si-0.45%Mg alloy under the conditions: a) as centrifuged; b) 255°C/30 min; c) 300°C/30 min; d) 255°C/90 min; and e) 300°C/90 min.

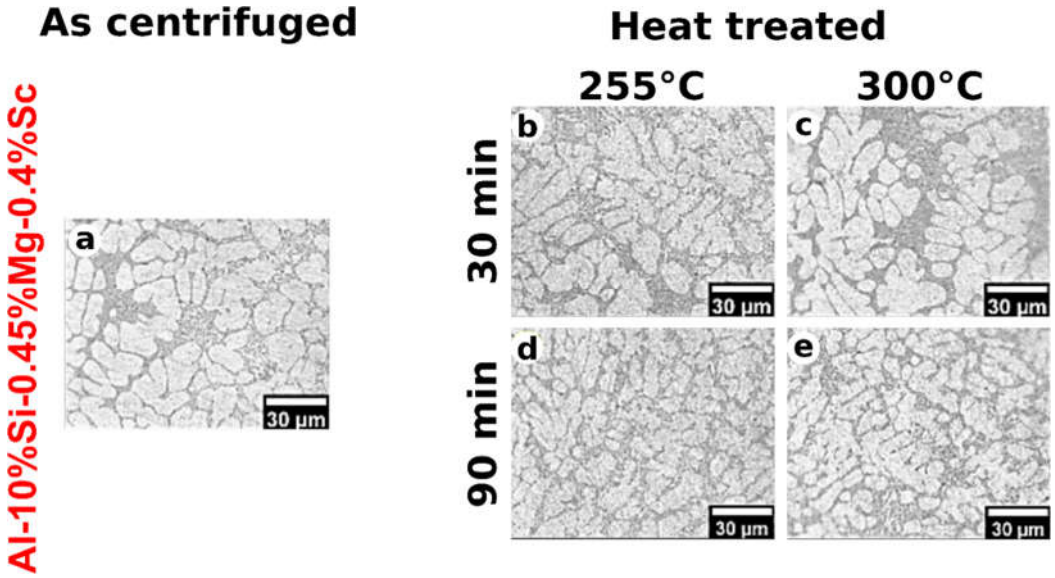

Figure 4. Representative microstructures of the Al-10%Si-0.45%Mg-Sc alloy under the conditions: a) as centrifuged; b) 255°C/30 min; c) 300°C/30 min; d) 255°C/90 min; and e) 300°C/90 min.

Both alloys were able to maintain dendritic arrays with very fine dimensions after the aging treatment conditions, as measured by the dendritic spacings less than 8.3 µm in Figure 5. These alloys were processed based on centrifugal forces to cast the samples into a rotating Cu mold. This type of process tends to allow cooling rates between 102 and 103 K/s. The results of Gandolfi et al. [3] can be used to demonstrate the fast cooling obtained here. This study reported dendritic spacing of approximately 25 µm for a cooling rate of 10 K/s obtained by directional solidification of the AlSi10Mg alloy. This signifies that much higher solidification rates are required to achieve the finer spacings seen in the current results through centrifugal casting. Under such conditions, Sc addition was unable to decrease de dendrite arm spacing. This is in contrast to the findings of Pramod et al.

Preprints (www.preprints.org) | NOT PEER-REVIEWED | Posted: 8 March 2023 doi:10.20944/preprints202303.0141.v1

[15] for the A356 alloy modified with Sc. The addition of 0.4 wt. %Sc reduced dendritic spacing by more than 50% (from 23m to 10m). In this case, slow solidification was practiced by using a pre-heated graphite mold to 200°C.

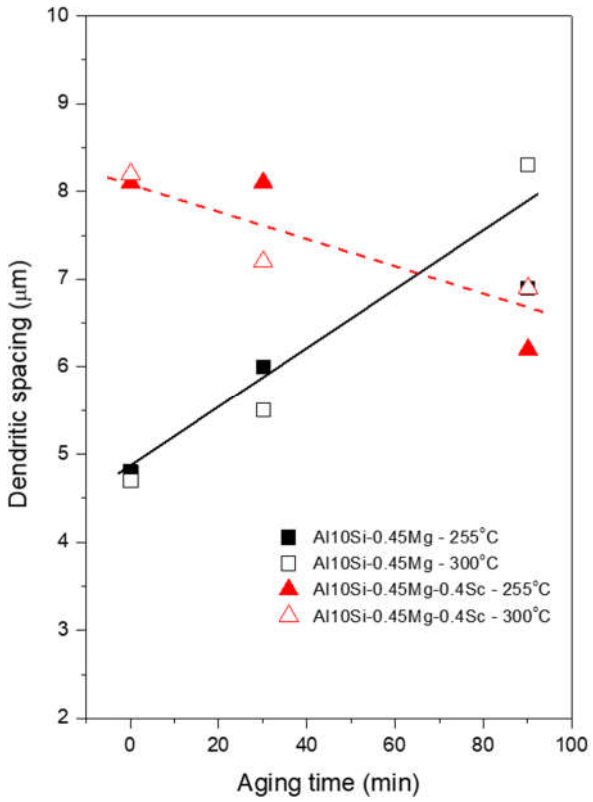

Figure 5. Dendritic spacing values for Al-10%Si-0.45%Mg and Al-10%Si-0.45%Mg-0.4%Sc alloy samples before and after aging at two temperatures.

Given the importance of dendritic scale as a hardening factor for Al-Mg-Si alloys, understanding the effect of Sc on dendritic spacing and variations during aging are critical aspects that have not been addressed for these alloys in the specialized literature. While processes such as grain size and precipitate size have been thoroughly investigated during heat treatment of Al-Mg-Si alloys [16–18], the variation in size of the Al-rich dendritic phase is little known under aging, and it has the potential to affect the properties as well.

Although the standard deviations associated with dendritic spacing measurements were approximately 1.3 μm, causing the data set deviations to be relatively large, Figure 5 depicts the evolution of mean dendritic spacing values as a function of aging time. Dendritic coarsening was clearly noted in the Al-Si-Mg alloy samples, in which spacing varied from 4.7 μm to 8.3 μm if compared to the as-cast with the 90min/300°C-aged samples. The diffusion process, which stimulates the migration of atoms from dendritic contours to neighboring dendrites, governs this growth for the AlSi10Mg alloy [19].

Aging heat treatment entails heating the material to a specific temperature and maintaining it for a set period of time, which takes last hundreds of minutes. The heat treatment deals with the acceleration of the diffusion process, which would naturally occur at room temperature over a much longer time period. In this context, microstructural changes can be observed when a solidified as-cast structure composed of dendrites is subjected to a thermal cycle (temperature and time) if the temperature and time are sufficient. Thermally activated dendritic array expansion is defined as the growth of certain dendrites at the expense of others in order to reduce the total area of the dendritic contours.

In contrast, the dendritic spacing related to the Sc-containing alloy was little affected by the aging time. For example, comparing the dendritic spacing for 30 min and for 90 min at 300°C gives 7.2 μm

Preprints (www.preprints.org) | NOT PEER-REVIEWED | Posted: 8 March 2023 doi:10.20944/preprints202303.0141.v1

and 6.9 μm respectively (open triangles in Figure 5), with the dendritic array virtually unaffected by the aging process. Considering that the diffusion length is proportional to the square root of the mobility lifetime (t: s), the dendritic spacing results depend on $\sqrt{D_s \cdot t}$, being "Ds" the solid diffusion coefficient, m^2/s. Ds is of the order of 5×10^{-16} m^2 /s for Sc in Al [20] and of the order of 6×10^{-14} m2/s for Si in Al [21]. The two orders of magnitude lower coefficient for the Sc case appears to explain the dendritic growth inhibition observed in the Sc-containing alloy results in Figure 5.

3.3. XRD and SEM-EDS results

Figure 6 shows some typical XRD plots for both alloys under as-cast and as-aged conditions.

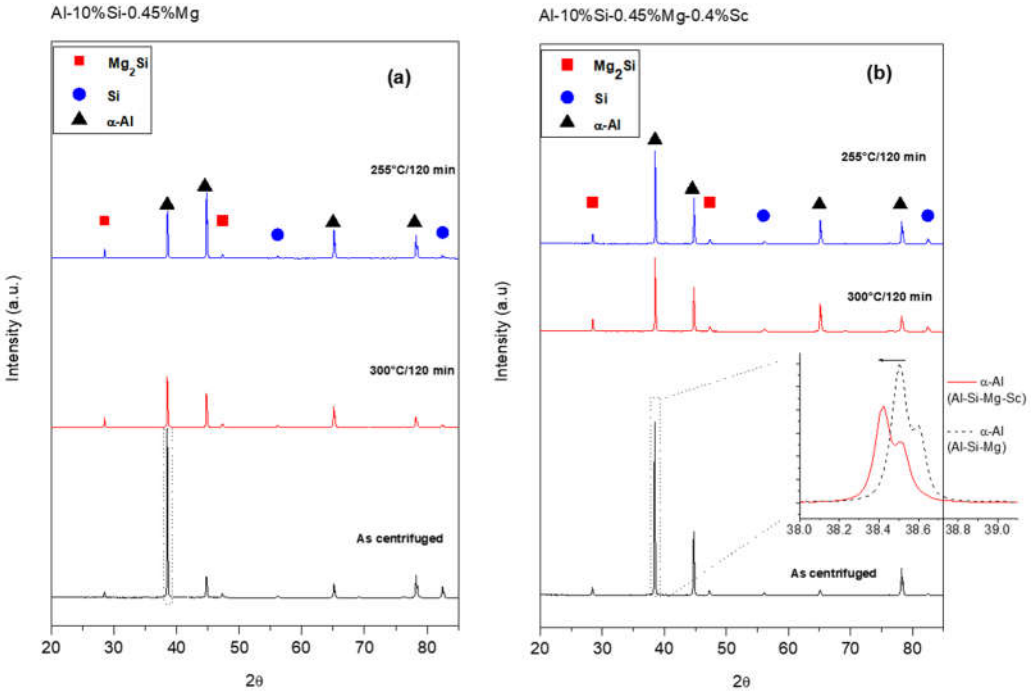

Figure 6. X-ray diffraction spectra of the as-centrifuged, 300°C/120min and 255°C/120min -aged samples: (a) Al-10%Si-0.45%Mg and (b) Al-10%Si-0.45%Mg-0.4%Sc alloys.

As illustrated in Figure 6, the X-ray diffraction analyses detected the α-Al, Si and Mg_2Si phases for all samples. Although the volume fraction referring to the Al_3Sc is too small and thus difficult to discern using X-ray diffraction, it appears that the presence of the Al_3Sc may cause the double peak associated with the α-Al phase (see extra pattern in Figure 6b). Harata et al. [22] identified peaks at approximately 38.5° for the Al_3Sc. The theorized similarity in the lattice parameters of Al and Al_3Sc justifies the effective nucleation action for solidification promoted by this phase [22].

When the reflections of the peaks corresponding to the decoded phases were examined, the Si 2θ values remained constant for all conditions without and with Sc. However, the -Al reflections differ if compared with both as-centrifuged samples, as illustrated in the supplement spectra inside Figure 6b. The Sc added Al-Si-Mg alloy may show an increase in the lattice parameter of α-Al phase which is clear evidence for the solid solution of Sc in α-Al [15]. Such Sc solubility in the primary α -Al matrix could be positive, resulting in Sc-rich precipitates and inherent age hardening upon annealing of the as-centrifuged samples.

The Sc-added samples tended to form increasingly larger precipitates when the alloy was exposed to longer aging times and temperatures. SEM-EDS mappings were performed, as shown in Figures 7 and 8, to demonstrate the element distributions and confirm the formed phases. While the Al_3Sc phase could not be confirmed in the as centrifuged samples, the formation of coarse Al_3Sc particles was observed in the most severe aging condition (300°C for 120 min). The Sc contrast in Figure 8 appears to indicate that the Al_3Sc phase precipitated during aging.

Preprints (www.preprints.org) | NOT PEER-REVIEWED | Posted: 8 March 2023 doi:10.20944/preprints202303.0141.v1

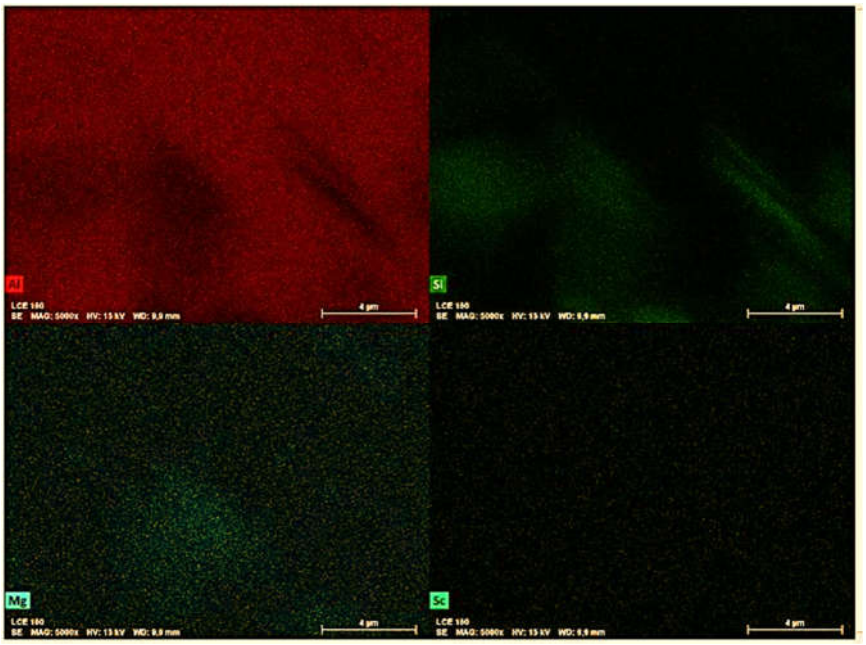

Figure 7. SEM-EDS images of the Al-10%Si-0.45%Mg-0.4%Sc alloy sample in the as-centrifuged condition.

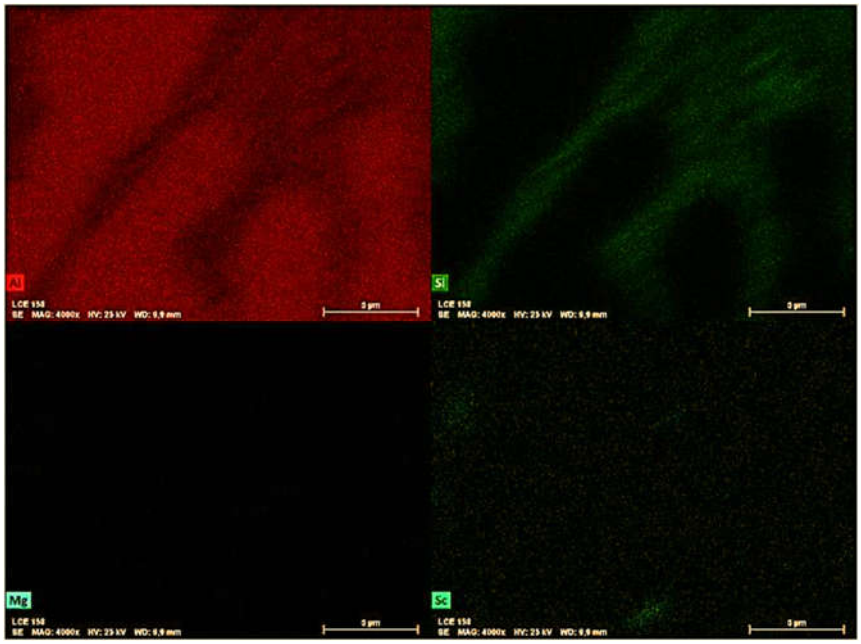

Figure 8. SEM-EDS images of the Al-10%Si-0.45%Mg-0.4%Sc alloy sample after heat treatment at 300°C for 120 min.

Sc has a maximum solubility of approximately 0.38 wt.% [16,23]. Fast cooling during solidification, on the other hand, makes it relatively simple to obtain higher supersaturated solutions of Sc in Al alloys, as evidenced by the XRD results. Under such quench conditions during the centrifugal cast, the self-aging can be performed immediately after the casting mold extraction (without the standard natural cooling, reheating, and solution heat-treatment, all prior to the quenching operation) [16]. In this context, the present research helps to advance the understanding of rapidly cooled structures and their subsequent self-aging in advanced manufacturing processes.

Binary Al-Sc alloys containing 0.1 wt.% Sc or more have previously demonstrated significant precipitation hardening [16,24]. However, the efficacy of adding Sc to commercial Al alloys remains to be determined. According to Røyset et al. [16], Sc precipitation hardening in non-heat treatable alloys may be more feasible. While some research has demonstrated the benefits of including Sc in

Preprints (www.preprints.org) | NOT PEER-REVIEWED | Posted: 8 March 2023 doi:10.20944/preprints202303.0141.v1

3xxx cast alloys [3,25]. For heat treatable alloys, Sc strengthening will be determined by the combined effect of small particle strengthening from Al_3Sc and strengthening from a refined grain/dendritic structure.

3.4. Vickers Hardness and STEM results

Figure 9 shows the average and standard deviation Vickers hardness values measured for the Al-10%Si-0.45%Mg and Al-10%Si-0.45%Mg-0.4%Sc alloys. It is possible to infer that the alloy samples with the Sc addition, in all cases, resulted in higher hardness. The samples with the highest hardness values for the two alloys are taken for comparison, that is, those thermally treated at 255°C for 60 minutes. In this case, there was an increase of approximately 13.5% from 97 HV to 110 HV due to adding Sc. This is most likely due to the influence of fine Sc precipitates, which cause precipitation hardening, whereas the dendritic array translated by a DAS of approximately 7 m in both samples has no significant effect on hardness.

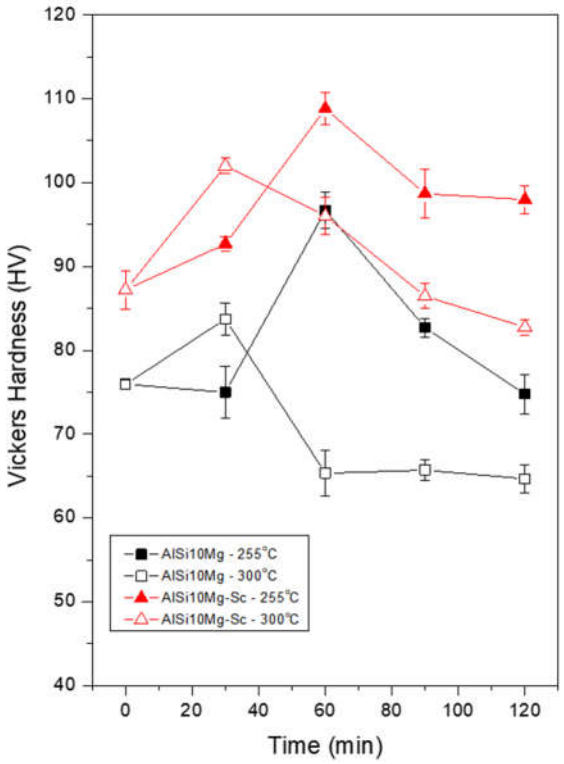

Figure 9. Vickers hardness of the as centrifuged Al-10%Si-0.45%Mg and Al-10%Si-0.45%Mg0.4%Sc alloys as well as of all aging conditions performed.

Furthermore, the clear importance of the relationship between time and optimal aging temperatures of aging of these alloys can be observed, as at 255°C, the hardness of both alloys benefited more from a longer treatment time, only presenting a drop when treated for 90 minutes. In contrast, while aged at 300°C there was a sharp drop in the hardness values as early as 60 minutes, indicating a possible excessive growth of the hardening precipitates.

STEM-EDS mapping was also used to identify the Sc-containing precipitates related to two different extreme conditions, i.e., 255°C/60 min (Figure 10) and 300°C/120 min (Figure 11). The Si phase has been identified as mainly showing fibrous morphology as seen in Figure 10. This appears to be mainly a result of the rapid solidification conditions that avoid the growth of Si plates due to the associated high cooling rate [26]. It seems that the conditions imposed during aging were not enough to either fragment or coarse the eutectic Si.

Preprints (www.preprints.org) | NOT PEER-REVIEWED | Posted: 8 March 2023 doi:10.20944/preprints202303.0141.v1

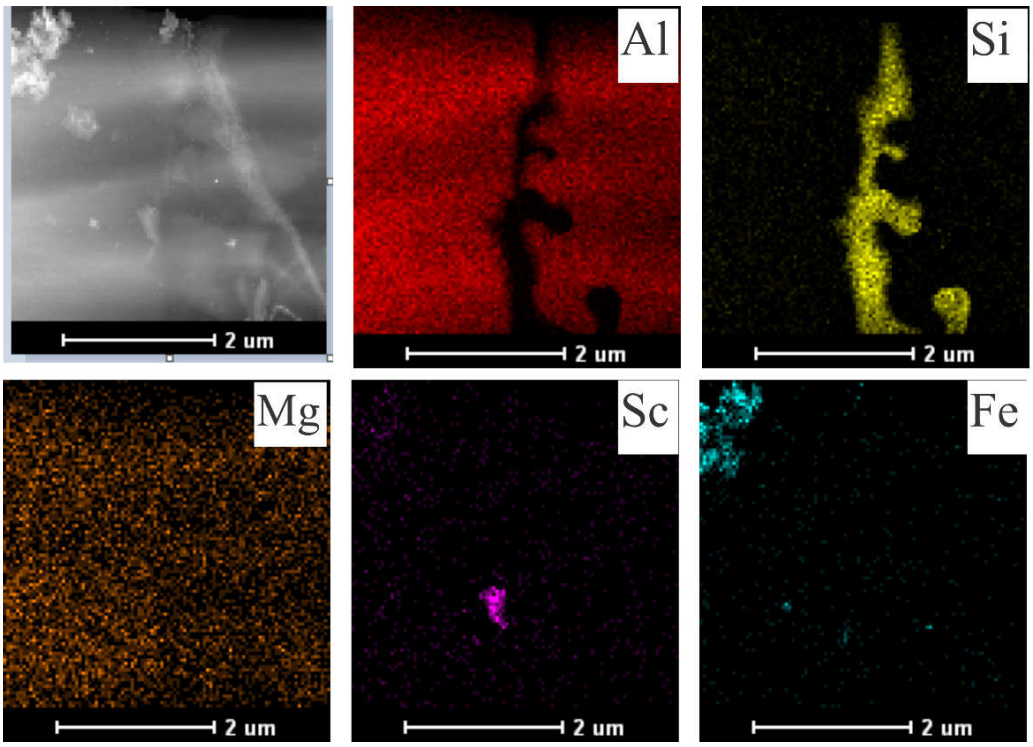

Figure 10. HAADF-STEM image and Al, Si, Mg, Fe, and Sc EDS maps of the Al-10%Si-0.45%Mg-Sc alloy aged at 255°C for 60 min.

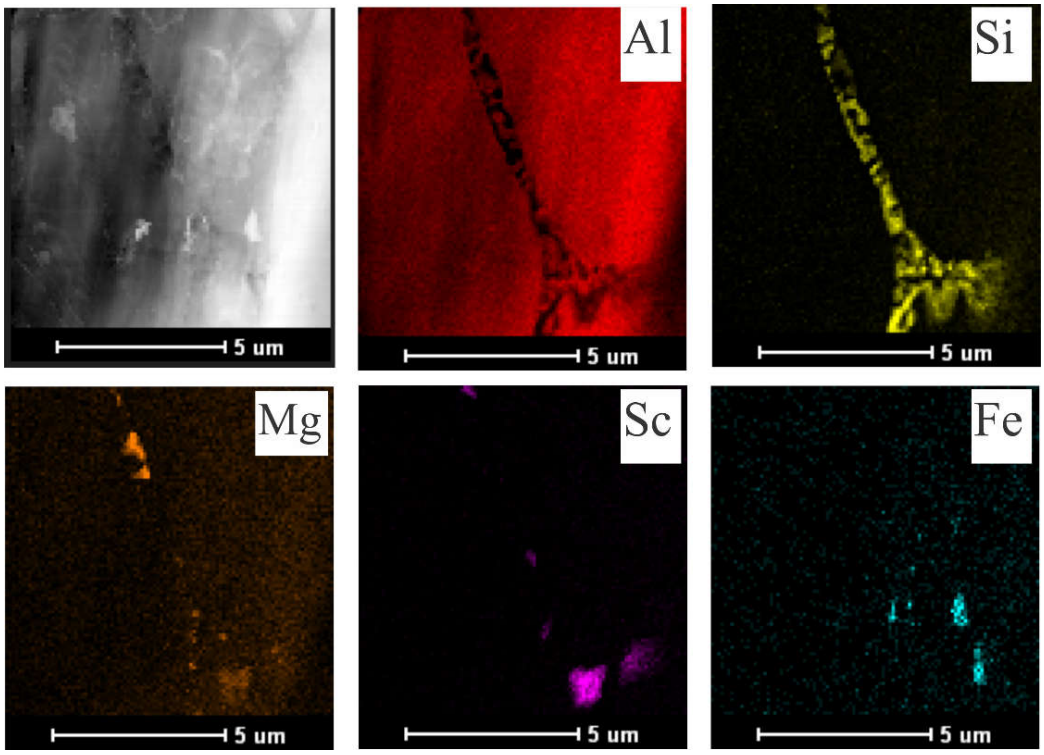

Figure 11. HAADF-STEM image and Al, Si, Mg, Fe, and Sc EDS maps of the Al-10%Si-0.45%Mg-Sc alloy aged at 300°C for 120 min.

There were a few Fe-bearing particles in the α-Al matrix. Furthermore, Mg-rich particles appear to be uniformly distributed, with some Mg- and Sc-rich clusters appearing to be interconnected, as observed by Spierings et al. [27]. The elemental EDS maps display the Sc-containing precipitates within the -Al matrix. It can be seen that higher time and temperature promoted the growth of these

 doi:10.20944/preprints202303.0141.v1

precipitates (Figure 11). In contrast, relatively small precipitates (100-200 nm) within the α-Al matrix could be observed for the 255°C/60min aged sample.

Chen et al. [2] also demonstrated that small addition of Sc has a positive impact on the hardness of 0.3wt.% Sc-modified AlSi10Mg alloys due to precipitation of finely dispersed Al_3Sc particles. Furthermore, these authors demonstrated that lower aging temperatures (225°C) are more effective in achieving higher hardness than 275°C and 325°C.

The current study demonstrated that direct aging of a rapidly solidified AlSi10Mg(-Sc) alloy is a time and cost-efficient processing method. As a result, if the proper aging conditions are met, Sc as an addition may be beneficial, particularly for rapidly solidified samples produced by processes such as die-casting, centrifugal casting, atomization, and additive manufacturing.

4. Conclusions

Dendritic spacings were measured for the investigated Al-Si-Mg alloys with and without Sc in non-treated and treated samples at various stages of precipitation. Furthermore, Vickers hardness values were mapped. The formed phases were identified and their effects on hardness were discussed. Optimized temperature and conditions for the direct aging of the AlSi10Mg alloy modified with Sc are proposed, with the following conclusions:

- After 90 min at 300°C, the dendritic spacing in the Al-10wt.%Si-0.45wt.%Mg samples nearly doubled. In contrast, the aging time had little effect on the dendritic spacing of the Sc-containing alloy;
- Aging treatments carried out at 300°C required a shorter time to reach a peak hardness value and showed the best hardness values for a period of 30 min. However, if the treatment time was extended, the hardness values decreased sharply. For the aging carried out at 255°C for 30 min., a strong hardness decrease was not observed, but the highest hardness values during aging were also not attained;
- The Vickers hardness values of the Sc-containing alloy were higher than those noted for the Al-10%Si-0.45%Mg alloy, indicating a hardening effect related to the formation of Al_3Sc precipitates, probably combined with the hardening effects of precipitates typically form in the conventional Al-Si-Mg alloy, such as β' and β'';
- The Vickers hardness of the Sc-containing alloy can deteriorate from high temperatures and lengthy treatments. This was because under these conditions, larger Sc-bearing precipitates having approximately 1 μm in size grew, having a less pronounced hardening impact. The best aging condition was demonstrated as being 255°C for 60 min. A very fine dispersion of precipitates (200 nm in size) was produced with a peak hardness of 110 HV.

Author Contributions: Conceptualization, J.S.; methodology, F.M., G.G., C.S., J.L.; formal analysis, J.S, G.G.; investigation, F.M., A.S., G.G.; resources, J.S.; data curation, F.F., G.G., J.L.; writing, G.G., J.S., writing—review and editing, G.G.; visualization, F.M., A.S.; supervision, J.S., G.G.; project administration, J.S., G.G.; funding acquisition, J.S.

Data Availability Statement: Data presented in this study are available on request from the corresponding author. Data are not publicly available because they pertain to a research still in development.

Acknowledgements: The authors acknowledge FAPESP (grants #2019/23673-7, # 2019/21937-7, and #2021/08436-9) and CNPq. This study was financed in part by the Coordenação de Aperfeiçoamento de Pessoal de Nível Superior - Brasil (CAPES) - Finance Code 001.

Conflicts of Interest: The authors declare no conflict of interest.

References

1. Giovagnoli, M.; Tocci, M.; Fortini, A.; Merlin, M.; Ferroni, M.; Migliori, A.; Pola, A. Effect of Different Heat-Treatment Routes on the Impact Properties of an Additively Manufactured AlSi10Mg Alloy. *Materials Science and Engineering A* **2021**, *802*, doi:10.1016/j.msea.2020.140671.

2. Chen, Y.; Wang, L.; Feng, Z.; Zhang, W. Effects of Heat Treatment on Microstructure and Mechanical Properties of SLMed Sc-Modified AlSi10Mg Alloy. *Progress in Natural Science: Materials International* **2021**, *31*, 714–721, doi:10.1016/j.pnsc.2021.08.003.
3. Gandolfi, M.; Xavier, M.G.C.; Gomes, L.F.; Reyes, R.A.V.; Garcia, A.; Spinelli, J.E. Relationship between Microstructure Evolution and Tensile Properties of Alsi10mg Alloys with Varying Mg Content and Solidification Cooling Rates. *Metals (Basel)* **2021**, *11*, doi:10.3390/met11071019.
4. Peng, Z.; Cui, L.; He, D.; Guo, X.; Zeng, Y.; Cao, Q.; Huang, H. Effect of Er and Zr Addition on Laser Weldability of AlSi10Mg Alloys Fabricated by Selective Laser Melting. *Mater Charact* **2022**, *190*, doi:10.1016/j.matchar.2022.112070.
5. Silbernagel, C.; Ashcroft, I.; Dickens, P.; Galea, M. Electrical Resistivity of Additively Manufactured AlSi10Mg for Use in Electric Motors. *Addit Manuf* **2018**, *21*, 395–403, doi:10.1016/j.addma.2018.03.027.
6. Tan, Q.; Yin, Y.; Fan, Z.; Zhang, J.; Liu, Y.; Zhang, M.X. Uncovering the Roles of LaB6-Nanoparticle Inoculant in the AlSi10Mg Alloy Fabricated via Selective Laser Melting. *Materials Science and Engineering A* **2021**, *800*, doi:10.1016/j.msea.2020.140365.
7. Li, Q.; Qiu, F.; Dong, B.X.; Yang, H.Y.; Shu, S.L.; Zha, M.; Jiang, Q.C. Investigation of the Influences of Ternary Mg Addition on the Solidification Microstructure and Mechanical Properties of As-Cast Al–10Si Alloys. *Materials Science and Engineering A* **2020**, *798*, doi:10.1016/j.msea.2020.140247.
8. Li, R.; Wang, M.; Yuan, T.; Song, B.; Chen, C.; Zhou, K.; Cao, P. Selective Laser Melting of a Novel Sc and Zr Modified Al-6.2 Mg Alloy: Processing, Microstructure, and Properties. *Powder Technol* **2017**, *319*, 117–128, doi:10.1016/j.powtec.2017.06.050.
9. Stadler, F.; Antrekowitsch, H.; Fragner, W.; Kaufmann, H.; Uggowitzer, P.J. Effect of Main Alloying Elements on Strength of Al–Si Foundry Alloys at Elevated Temperatures. *International Journal of Cast Metals Research* **2012**, *25*, 215–224, doi:10.1179/1743133612Y.0000000004.
10. Fang, L.; Zhang, X.; Hu, H.; Nie, X.; Tjong, J. Microstructure and Tensile Properties of Squeeze Cast Aluminium Alloy A380 Containing Ni and Sr Addition. *Advances in Materials and Processing Technologies* **2017**, *3*, 90–100, doi:10.1080/2374068X.2016.1247341.
11. Yakubov, V.; He, P.; Kruzic, J.J.; Li, X. Precipitate Formation in Cerium-Modified Additively Manufactured AlSi10Mg Alloy. *Australian Journal of Mechanical Engineering* **2021**, doi:10.1080/14484846.2021.1997133.
12. Henein, H.; Bogno, A.A.; Yin, S.; Natzke, P.; Gallerneault, M. On the Role of Sc in Powders and Spray Deposits of Hypoeutectic Al-Cu: À Propos Du Rôle de Sc Dans Les Poudres et Les Revêtements Par Projection d'Al-Cu Hypoeutectique. *Canadian Metallurgical Quarterly* **2022**, doi:10.1080/00084433.2022.2095138.
13. Stunová, B.B. Strontium as a Structure Modifier for Non-Binary Al-Si Alloy. *Acta Polytechnica* **2012**, *52*, 26–32, doi:10.14311/1580.
14. Marquis, E.A.; Seidman, D.N.; Dunand, D.C. Effect of Mg Addition on the Creep and Yield Behavior of an Al-Sc Alloy. *Acta Mater* **2003**, *51*, 4751–4760, doi:10.1016/S1359-6454(03)00288-X.
15. Pramod, S.L.; Ravikirana; Rao, A.K.P.; Murty, B.S.; Bakshi, S.R. Effect of Sc Addition and T6 Aging Treatment on the Microstructure Modification and Mechanical Properties of A356 Alloy. *Materials Science and Engineering A* **2016**, *674*, 438–450, doi:10.1016/j.msea.2016.08.022.
16. Røyset, J.; Ryum, N. Scandium in Aluminium Alloys. *International Materials Reviews* **2005**, *50*, 19–44, doi:10.1179/174328005X14311.
17. Zhang, J.; Feng, J.; Zuo, L.; Ye, B.; Kong, X.; Jiang, H.; Ding, W. Effect of Sc Microalloying Addition on Microstructure and Mechanical Properties of As-Cast Al–12Si Alloy. *Materials Science and Engineering A* **2019**, *766*, doi:10.1016/j.msea.2019.138343.
18. Dorin, T.; Ramajayam, M.; Babaniaris, S.; Jiang, L.; Langan, T.J. Precipitation Sequence in Al–Mg–Si–Sc–Zr Alloys during Isochronal Aging. *Materialia (Oxf)* **2019**, *8*, doi:10.1016/j.mtla.2019.100437.
19. Sadeghi, I.; Wells, M.A.; Esmaeili, S. Modeling Homogenization Behavior of Al-Si-Cu-Mg Aluminum Alloy. *Mater Des* **2017**, *128*, 241–249, doi:10.1016/j.matdes.2017.05.006.
20. Kerkove, M.A.; Wood, T.D.; Sanders, P.G.; Kampe, S.L.; Swenson, D. The Diffusion Coefficient of Scandium in Dilute Aluminum-Scandium Alloys. *Metall Mater Trans A Phys Metall Mater Sci* **2014**, *45*, 3800–3805, doi:10.1007/s11661-014-2275-4.
21. Fujikawa, S.; Hirano, K.; Fukushima, Y. Diffusion of Silicon in Aluminum. *Metallurgical Transactions A* **1978**, *9*, 1811–1815, doi:10.1007/BF02663412.

22. Harata, M.; Yasuda, K.; Yakushiji, H.; Okabe, T.H. Electrochemical Production of Al–Sc Alloy in CaCl2–Sc2O3 Molten Salt. *J Alloys Compd* **2009**, *474*, 124–130, doi:10.1016/j.jallcom.2008.06.110.
23. Røyset, J.; Ryum, N. Kinetics and Mechanisms of Precipitation in an Al-0.2wt.% Sc Alloy. *Materials Science and Engineering A* **2005**, *396*, 409–422, doi:10.1016/j.msea.2005.02.015.
24. Seidman, D.N.; Marquis, E.A.; Dunand, D.C. Precipitation Strengthening at Ambient and Elevated Temperatures of Heat-Treatable Al(Sc) Alloys. *Acta Mater* **2002**, *50*, 4021–4035, doi:10.1016/S1359-6454(02)00201-X.
25. Lim, Y.P.; Yeo, W.H. The Effects of Scandium on A356 Aluminium Alloy in Gravity Die Casting. *Materials Research Innovations* **2014**, *18*, S6-395-S6-399, doi:10.1179/1432891714Z.000000000985.
26. Hosch, T.; England, L.G.; Napolitano, R.E. Analysis of the High Growth-Rate Transition in Al-Si Eutectic Solidification. *J Mater Sci* **2009**, *44*, 4892–4899, doi:10.1007/s10853-009-3747-6.
27. Spierings, A.B.; Dawson, K.; Heeling, T.; Uggowitzer, P.J.; Schäublin, R.; Palm, F.; Wegener, K. Microstructural Features of Sc- and Zr-Modified Al-Mg Alloys Processed by Selective Laser Melting. *Mater Des* **2017**, *115*, 52–63, doi:10.1016/j.matdes.2016.11.040.